

# Panoramic Distortion-Aware Tokenization for Person Detection and Localization Using Transformers in Overhead Fisheye Images

Nobuhiko Wakai<sup>1</sup> Satoshi Sato<sup>1</sup> Yasunori Ishii<sup>1</sup> Takayoshi Yamashita<sup>2</sup>

<sup>1</sup> Panasonic Holdings Corporation <sup>2</sup> Chubu University

{wakai.nobuhiko,sato.satoshi,ishii.yasunori}@jp.panasonic.com

takayoshi@isc.chubu.ac.jp

## Abstract

Person detection methods are used widely in applications including visual surveillance, pedestrian detection, and robotics. However, accurate detection of persons from overhead fisheye images remains an open challenge because of factors including person rotation and small-sized persons. To address the person rotation problem, we convert the fish-eye images into panoramic images. For smaller people, we focused on the geometry of the panoramas. Conventional detection methods tend to focus on larger people because these larger people yield large significant areas for feature maps. In equirectangular panoramic images, we find that a person’s height decreases linearly near the top of the images. Using this finding, we leverage the significance values and aggregate tokens that are sorted based on these values to balance the significant areas. In this leveraging process, we introduce panoramic distortion-aware tokenization. This tokenization procedure divides a panoramic image using self-similarity figures that enable determination of optimal divisions without gaps, and we leverage the maximum significant values in each tile of token groups to preserve the significant areas of smaller people. To achieve higher detection accuracy, we propose a person detection and localization method that combines panoramic-image remapping and the tokenization procedure. Extensive experiments demonstrated that our method outperforms conventional methods when applied to large-scale datasets.

## 1. Introduction

In the commercial and industrial fields, object detection methods are used in a wide range of applications, including visual surveillance [10, 22, 61, 66], pedestrian detection [6, 18, 68], and robots [20, 64, 67]. In particular, the spotlight on fisheye person detection has been growing because of its various applications, from monitoring of public transportation and infrastructure to worker movement optimization in factories, and player movements analysis for

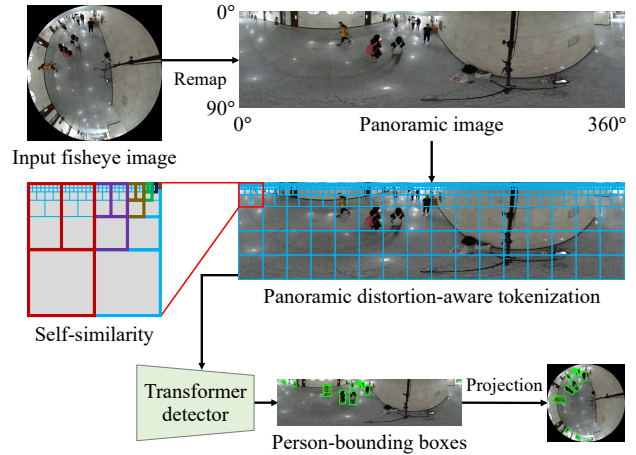


**Figure 1.** Our method converts an overhead fisheye image into an equirectangular panoramic image by remapping. This panoramic image is then divided using a distortion-aware tokenization process based on self-similarity figures using a unit figure, which is colored dark red and consists of a square and two rectangles. Our transformer-based detector uses the resulting tokens to detect person-bounding boxes within the panoramic image. We then obtain the bounding boxes in the fisheye images from the panoramic image via projection. The input image is taken from [63].

sports strategy. Overhead fisheye cameras are suitable for use in these applications because they are omnidirectional and have a larger field of view than conventional narrow-view cameras; *i.e.*, one overhead fisheye camera can be substituted for several narrow-view cameras. However, the overhead fisheye images do not match the inputs of the detectors [12, 58, 72], which requires perspective images. This mismatch is derived from person rotation and the presence of small-sized people in the images. The person rotation factor leads to individual persons having various shapes and appearances in the fisheye images. Within the near image circle of circumferential fisheye images, smaller people are captured at a long distance from the fisheye cameras. Although person detection methods based on use of narrow-view cameras are well-established, deriving accurate tech-

**Table 1.** Comparison of the features of conventional methods and with those of our proposed method

Method	Detector <sup>1</sup>	Training	Bounding box	Core idea to address	
				Person rotation	Small person
CNN-based					
Seidel <i>et al.</i> [40]	VISAPP'19	YOLOv2 [34]	Orthogonal rectangle	✓	
Li <i>et al.</i> [21]	AVSS'19	YOLOv3 [35]	Rotated rectangle	✓	
Tamura <i>et al.</i> [46]	WACV'19	YOLOv2 [34]	Rotated rectangle	✓	
RAPiD [9]	CVPRW'20	Feature pyramid network [24]	Rotated rectangle	✓	
OARPD [33]	MTA'24	YOLOv8 [51]	Rotated rectangle	✓	
Transformer-based					
Yang <i>et al.</i> [63]	ICCV'23	DAB-DETR [26]	Rotated rectangle	✓	
Ours		DAB-DETR [26]	Rotated trapezoid	✓	✓

<sup>1</sup> Each detector was modified to address overhead fisheye images.

niques for person detection and localization from overhead fisheye images has remained an open challenge.

Person detection methods have been proposed that used convolutional neural networks (CNNs) [19] and transformers [52] to analyze overhead fisheye images. Early CNN-based methods [21, 40] used detectors that were trained on perspective images. To improve the performance of both the CNN-based methods [9, 33, 46] and a transformer-based method [63], their training was also conducted using overhead fisheye images. However, it is difficult for these conventional methods to detect people accurately in overhead fisheye images because of the rotation and small person size problems mentioned above.

Based on the observations above, to realize accurate person detection, we propose a transformer-based method that detects rotated bounding boxes from an overhead fisheye image, as illustrated in Figure 1. An input fisheye image is converted into a panoramic image using a remapping method. For the panoramic image, we introduce a tokenization method called panoramic distortion-aware tokenization (PDAT) to balance the significant areas of feature maps. This tokenization uses self-similarity figures to perform nonuniform divisions by matching the token tile size with a person’s height; *i.e.*, the height depends on the vertical image coordinates of the panoramic image. Finally, we obtain bounding boxes in the fisheye images via projection.

To investigate the effectiveness of these proposed methods, we conducted extensive experiments on a large-scale dataset [63]. This evaluation demonstrated that our proposed method outperforms both the conventional CNN-based [9, 21, 33, 40, 46] and transformer-based [63] methods. The major contributions of our study are summarized as follows:

- We propose a transformer-based method for person detection and localization in overhead fisheye images to achieve higher accuracy than the conventional methods without the need to balance significant areas of the feature maps.
- We introduce the PDAT method with optimal divisions

based on self-similarity figures to address a person’s height using the vertical panoramic-image coordinates.

## 2. Related work

**Overhead-fisheye-image person detection.** Person detection techniques in overhead fisheye images have been developed using large-scale datasets [5, 9, 21, 47, 63]. Existing person detection methods for overhead fisheye images can be classified into two categories: CNN-based and transformer-based methods, as listed in Table 1. Seidel *et al.* [40] proposed a pioneering CNN-based detection method. The method divides a fisheye image into upright image patches that are undistorted using the given camera parameters. Although the patches are perspective images, the method requires camera calibration before detection. Li *et al.* [21] proposed a CNN-based method to improve detection accuracy using focal windows that can extract upright images. Tamura *et al.* [46] proposed a method that uses YOLOv2 [34], which had been trained on perspective images from the COCO dataset [23], using rotation augmentation. To train a detector called RAPiD, Duan *et al.* [9] introduced the angle-aware loss function. Inspired by the RAPiD detector being trained on fisheye images, OARPD [33] was proposed with use of the center distance intersection over union approach to address rotated bounding boxes. Yang *et al.* [63] proposed a pioneering transformer-based method with rotation-equivariant training. For a query-based detector, this training strategy involves use of an additional query of a 90°-rotated image to tackle rotated persons. Both the CNN-based and transformer-based methods described above focused primarily on person rotations. Although both the CNN-based and Transformer-based methods can detect people, images containing people of various sizes cause performance degradation.

**Panoramic-image conversion.** When the camera parameters are given, the panoramic images, fisheye images, and spherical representations are all convertible. This conversion method can be applied in various tasks using fish-

eye and panoramic images. To alleviate fisheye distortion, Plaut *et al.* [32] converted fisheye images into equirectangular images to perform 3D object detection. In deep single image camera calibration, equirectangular images were converted into fisheye images to perform dataset generation [28, 54]. Furthermore, Wang *et al.* [56] used spherical representations taken from equirectangular images to perform 360° room layout estimation. As described in the discussion of overhead-fisheye-image person detection above, conventional methods do not convert the fisheye images into panoramic images because person detection in panoramic images remains an open challenge.

**Small object detection.** Object detection accuracy tends to decrease for smaller objects. Small objects are often captured at long distances, *e.g.*, in a dataset acquired using a drone [70]. Small object detection methods are generally classified into three categories: division-based methods, augmentation-based methods, and enlargement-based methods. The division-based methods involve multi-scale training performed using image pyramids [43], image cropping [44], and feature pyramids [13]. The augmentation-based methods [12, 65] were proposed to realize data invariance. The enlargement-based methods enlarge the input images [25, 50, 57] and conduct super-resolution processing [16, 42]. The methods noted above do not use the prior knowledge that smaller people are only located near the image circles in overhead fisheye images. Therefore, these conventional methods do not work effectively for person detection in overhead fisheye images.

**Visual localization.** Various localization methods have been established to determine either camera poses or person locations from an image. Visual localization methods can be classified into three categories: query-based methods, regression-based methods, and geometry-based methods. The query-based methods estimate camera poses using databases composed of geo-tagged images [1, 3, 15, 39, 48, 62] and 3D scene structure models [11, 38]. Before query-based methods can be used, the databases and models must first be built in a time-consuming process. The regression-based methods [17, 55] can estimate camera poses without the need for databases and models; however, their inferences can only be applied to the same scenes that were used for training. More recently, Yang *et al.* [63] introduced a pioneering geometry-based method for use with overhead fisheye images.

Yang *et al.*'s localization method [63] estimates person locations based on the camera geometry after camera calibration. The camera models express the required mapping from world coordinates  $\tilde{\mathbf{p}}$  to image coordinates  $\tilde{\mathbf{u}}$  in homo-

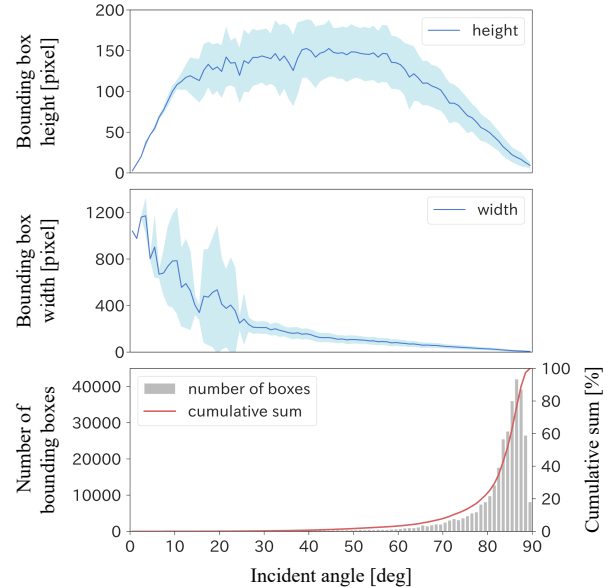


**Figure 2.** Distribution of the bounding boxes on the LOAF training set. This distribution was analyzed using incident angles at 1°-intervals based on the center of the bounding boxes. The first and second rows represent the mean heights and widths of the bounding boxes in a panoramic image with 2048×512 pixels, respectively. The cyan regions indicate the standard deviations in each bin of incident angles. The bottom image shows the number of bounding boxes.

geneous coordinates. This mapping is represented as

$$\tilde{\mathbf{u}} = \begin{bmatrix} \gamma/d_u & 0 & c_u \\ 0 & \gamma/d_v & c_v \\ 0 & 0 & 1 \end{bmatrix} [\mathbf{R} \mid \mathbf{t}] \tilde{\mathbf{p}}, \quad (1)$$

where  $\gamma$  is the distortion,  $(d_u, d_v)$  is the image sensor pitch,  $(c_u, c_v)$  is a principal point,  $\mathbf{R}$  is a rotation matrix, and  $\mathbf{t}$  is a translation vector. The subscripts of  $u$  and  $v$  denote the horizontal and vertical directions, respectively. Given the camera parameters used in Equation (1), we can determine the 3D vector of the incident ray from  $\tilde{\mathbf{u}}$ . The line that passes through a camera along the incident ray vector crosses the ground plane. Therefore, we can calculate the distance between the crossing point and the ground point beneath the camera for a person when  $\tilde{\mathbf{u}}$  represents the center of a detected person-bounding box. However, accurate person detection is essential because the estimated location is sensitive to person detection errors. We therefore focused on geometry-based localization; *i.e.*, the process is adapted to surveillance using overhead fisheye cameras.

**Transformer tokenization.** Dosovitskiy *et al.* [8] proposed a pioneering transformer-based method using a tokenization approach that divides an input image into square patches. Numerous tokenization methods have been proposed to date because these square patches lead to high

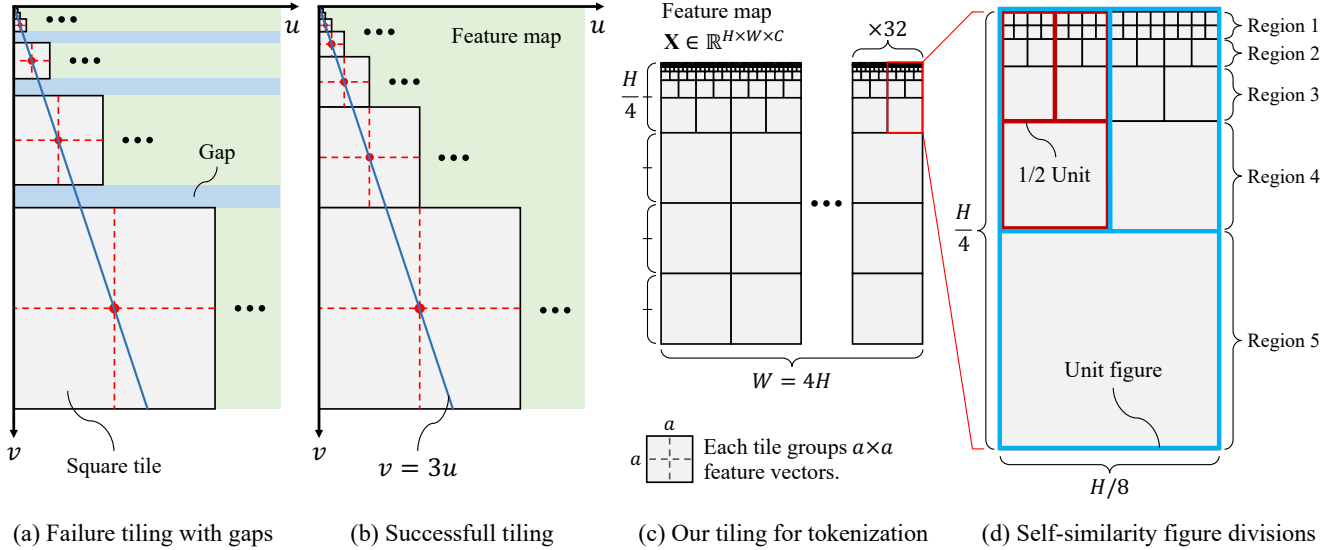


**Figure 3.** Panoramic distortion-aware tokenization. The tiling examples indicate tiling failure with gaps and successful tiling in (a) and (b), respectively. The blue lines through the tile centers, where  $v = 3u$ , indicate that the heights of the tiles change linearly. (c) Our tiling for tokenization method fills a feature map. (d) The unit figure of the self-similarity figure divisions is indicated when the number of regions  $K$  is five.

computational costs. Window-based methods focus on the token groups using shifted windows [27], cross-shaped windows [7], dilated windows [49, 59], and scalable sliding windows [14]. In contrast to static window shapes, deformable attention methods [60] were proposed to improve flexibility. To address the problem of multiple tokens being generated in unimportant regions, *e.g.*, in the background, BiFormer [69] prunes the regions using a coarse-to-fine strategy, and SG-Former [36] aggregates the regions. Although the methods described above are all well-developed, these methods were designed for use with perspective images. For fisheye image applications, DarSwin [2], which uses radial patches formed by polar partitioning, was proposed. However, this partitioning approach is not suitable for person detection in overhead fisheye images because a small number of the relevant tokens are generated in near image circles.

### 3. Proposed method

In this section, we first analyze the bounding boxes in an overhead fisheye dataset. Second, we introduce PDAT and depict how it groups the tokens. Third, we describe our transformer-based method for person detection and localization using PDAT. Finally, we describe our training and inference phases.

#### 3.1. Analysis of overhead fisheye dataset

The geometric relationship between equirectangular images and overhead fisheye cameras leads to the fact that the

heights and widths of the bounding boxes decrease linearly when the incident angles are large enough. We verified the relationship using the LOAF training set, and Figure 2 shows the distribution of the bounding boxes along the different incident angles from the center of bounding boxes. This distribution indicates that the incident angles that are greater than approximately  $70^\circ$  satisfy the required relationship. In addition, the range of incident angles from  $80^\circ$  to  $90^\circ$  dominated 75% of the number of bounding boxes. Therefore, we design our tokenization method based on the relationship above, which we explain in further detail in the following.

#### 3.2. Panoramic distortion-aware tokenization

The goal of the PDAT is to match the person’s height with the height of the square tiles that group the tokens using nonuniformity divisions. As described in Section 3.1, the person’s height decreases linearly at incident angles exceeding  $70^\circ$ , corresponding to approximately the top of one-fourth of the height of the equirectangular images. Therefore, we align the square tiles, which have sizes that depend on the vertical axis  $v$ . We found that use of inappropriate tile sizes leads to gaps and use of consecutive half-sizes fills the feature maps, as shown in Figure 3(a) and (b), respectively. Our overall tiling method is illustrated in Figure 3(c). The top of the one-fourth of the image is occupied by performing consecutive half-size tiling, and the other three-fourths consist of tiles of the same size. Each of these tiles has  $a \times a$  of feature vectors, where  $a$  is the side length of the number of feature vectors in a single tile. As shown in Fig-

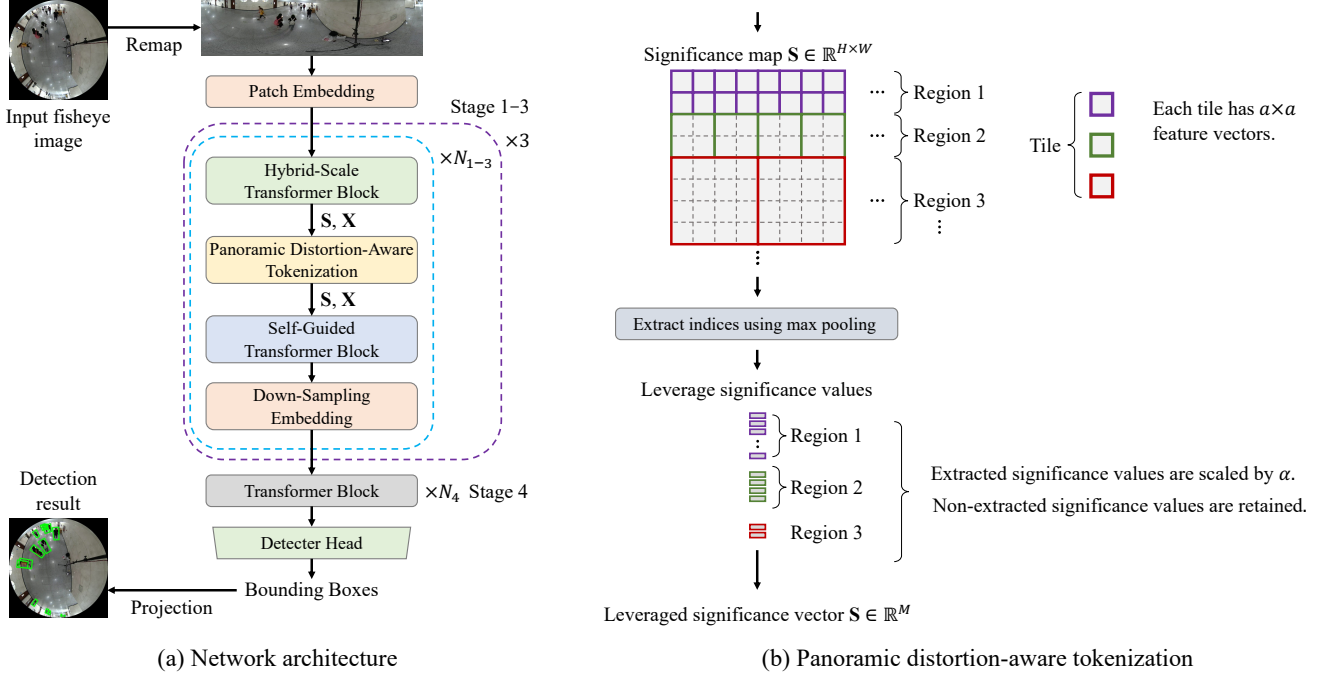


**Figure 4.** Overall proposed network architecture. (a) The network architecture has a detector head and a backbone consisting of four stages. The  $N$  indicates the number of blocks in the subscript stage. (b) The panoramic distortion-aware tokenization process aggregates the significance map  $S$  and the feature map  $X$  using average pooling.

ure 3(d), our tiling is defined based on the self-similarity figures when using  $K$  regions, with the exception that the top two rows have tiles of the same size because we have used finite divisions. The unit figure consists of a square and two rectangles, and each rectangle can be divided recursively using another set composed of a square and two rectangles. Note that our division method was inspired by the Cantor ternary set [45], but our figure is not a fractal according to Mandelbrot’s definition [30]. Therefore, our tokenization method using self-similarity figures represents the optimal division in terms of matching the person’s height with the tile height.

### 3.3. Network architecture

**Panoramic-image conversion.** Our method converts an input fisheye image into an equirectangular panoramic image via remapping, as illustrated in Figure 1. When the input image is rectangular, we center-crop the image. To address any uncalibrated cameras, we assume that the input images represent the stereographic projection, which is a standard fisheye camera model. In the case of radial distortion, this projection uses a trigonometric function:  $\gamma = 2f_w \cdot \tan(\theta/2)$ , where  $f_w$  is the focal length and  $\theta$  represents the incident angles in Equation (1). We can then determine the focal length by fitting the image circle using  $90^\circ$  incident angles. The image coordinates  $\tilde{u}$  in the fisheye images are projected onto a unit sphere in world co-

ordinates  $\tilde{p}$  using backprojection [53], and then the world coordinates  $\tilde{p}$  are projected onto an equirectangular image with an arbitrary image width [41]. Note that we use the panoramic images with incident angles from  $0^\circ$  to  $90^\circ$  because the incident angle range from  $-90^\circ$  to  $0^\circ$  represents the directions behind the cameras.

**Transformer-based detector.** Following the approach in [63], we use the dynamic anchor box detection with transformers (DAB-DETR) [26] with the deformable attention mechanism [71], which has shown strong performance in object detection performances. Window-based transformers are not suitable for use in the backbone of DAT-DETR because PDAT divides the feature maps non-uniformly. Therefore, we use an aggregation-based transformer, SG-Former [36], for the backbone. Note that SG-Former is the only aggregation-based method of this type available. The proposed network architecture is shown in Figure 4(a). The detector head block represents DAB-DETR without the backbone, and the remaining blocks represent SG-Former and PDAT. The patch embedding is extracted using the CNN, and the transformer block is a vanilla transformer block [8]. The DAB-DETR method and the SG-Former follow the details given in the corresponding papers in the literature. We explain integration of PDAT into SG-Former in the following two steps: 1) SG-Former attention and 2) our tokenization details.

**SG-Former attention.** The core ideas of the SG-Former



are hybrid-scale self-attention and self-guided attention. The hybrid-scale attention process extracts both global and local information from a feature map  $\mathbf{X} \in \mathbb{R}^{H \times W \times C}$ , where  $H$ ,  $W$ , and  $C$  are the height, the width, and the channels of the map, respectively. To obtain the local information, the down-sampling is applied after the self-guided transformer blocks. The hybrid-scale attention process also calculates the significance map  $\mathbf{S} \in \mathbb{R}^{H \times W}$ , based on the feature map. For example, the face is a high-significance area and the background is a low-significance area. The self-guided attention process aims to aggregate the feature vectors based on the significance map. For example, the feature vectors in a high-significance area of the face are aggregated into half the number of feature vectors; in contrast, the feature vectors in a low-significance area of the background are aggregated into 1/28th feature vectors.

**Our tokenization details.** We aim to extend the self-guided attention process using PDAT. Our modification of SG-Former inserts PDAT between the hybrid-scale transformer block and the self-guided block. The PDAT then leverages the significance map  $\mathbf{S}$  based on the basis of feature vectors grouped by the tiles. This approach extends the self-guided attention process seamlessly. Figure 4(b) shows the PDAT pipeline. First, the significance maps are divided using our tiling method, as described in Section 3.2(c). From top to bottom, we split these maps horizontally into strips called regions. Second, we extract 2D max pooling indices for each region using square kernels of  $a \times a$  in each tile; *i.e.*, the kernel size is dependent on the regions. Finally, we leverage significance values extracted by max pooling. This leveraging in this case is that the significance values are multiplied by the scaling factor  $\alpha$ . This leveraging approach is designed to preserve the significance values of smaller people during aggregation of the feature vectors because larger people in the images yield multiple areas with high significance values. Therefore, our tokenization approach allows us to balance the significance values among people of various sizes.

### 3.4. Training and inference

**Training.** We generate equirectangular images from each training set. In this generation procedure, we avoid splitting the bounding boxes in the vertical image edges by changing the definition of the  $0^\circ$  pan angles. We then train our network using the panoramic images by following the training procedure given in [26].

**Inference.** First, we convert an input fisheye image into a panoramic image by a remapping process, as illustrated in Figure 4(a). Second, the panoramic image obtained is then fed into our network. Finally, we project the detected bounding boxes onto the fisheye image, on which the shape of each bounding box is a rotated trapezoid. This projection represents the backprojection from a fisheye image to a

**Table 2.** Properties of the LOAF dataset

Dataset	Resolution	Number of images			
		Train	Validation	Test	All
LOAF [63]	$1024 \times 1024$	29,569	4600	8773	42,942

panoramic image, as described in Section 3.3.

## 4. Experiments

To demonstrate the validity and effectiveness of our approach, we conducted extensive experiments using a large-scale dataset, LOAF [63], composed of overhead fisheye images in Table 2.

### 4.1. Parameter settings

For our network backbone, we used SG-Former-S [36] (where the backbone size is the smallest among the S, M, and B types), which was pretrained on ImageNet [37]. We trained our network using a mini-batch size of 8 and the AdamW optimizer [29]. The initial learning rate was set at  $2 \times 10^{-4}$  and was multiplied by 0.1 at the 40th epoch. We used the hyper-parameters of  $K = 5$ ,  $a = 3$ , and  $\alpha = 2$ . The remaining hyper-parameters were applied in [63]. Unless otherwise specified, panoramic images with  $3072 \times 768$  pixels were used.

### 4.2. Experimental results

We used the results of person detection and localization results reported by Yang *et al.* [63] in the methods of Seidel *et al.* [40], Li *et al.* [21], Tamura *et al.* [46], RAPiD [9], and Yang *et al.* [63]. We used the OARPD results reported in [33]. To acquire qualitative results, we used Yang *et al.*'s [63] official codes using PyTorch [31].

#### 4.2.1. Person detection

To demonstrate the validity and the effectiveness of the proposed method, we used the mean average precision (mAP) following a COCO evaluation [23]. Our method achieved the highest mAP among the methods listed in Table 3 on both the validation and test sets. The mAP in our method is substantially higher than that obtained using Yang *et al.*'s method [63] by values of 5.3 and 9.0 on the LOAF validation and test sets, respectively. Our method also achieved an  $AP_{seen}$  of 56.8 and an  $AP_{unseen}$  of 54.2 on the LOAF test set, thus outperforming the other methods. The substantial margin between our method and Yang *et al.*'s method [63] on the LOAF unseen test set was 9.3, which demonstrates scene robustness. In addition, our method outperformed the other methods on  $AP_n$  and our method demonstrated a performance comparable to that of Yang *et al.*'s method [63] on  $AP_m$  and  $AP_f$ .

**Table 3.** Person detection results using the average precision (AP)  $\uparrow$  on the LOAF validation (val) and test sets

Method	val						test										
	mAP	AP <sub>50</sub>	AP <sub>75</sub>	AP <sub>n</sub>	AP <sub>m</sub>	AP <sub>f</sub>	AP <sub>seen</sub>	AP <sub>unseen</sub>	mAP	AP <sub>50</sub>	AP <sub>75</sub>	AP <sub>n</sub>	AP <sub>m</sub>	AP <sub>f</sub>	AP <sub>seen</sub>	AP <sub>unseen</sub>	
Seidel <i>et al.</i> [40]	VISAPP'19	21.8	59.8	7.6	32.8	28.5	2.3	23.2	19.5	20.2	58.2	7.1	32.2	28.3	3.9	22.4	18.9
Li <i>et al.</i> [21]	AVSS'19	28.5	63.3	20.1	46.8	24.2	1.3	33.8	29.3	27.2	65.2	21.3	47.2	24.8	1.3	31.8	27.6
Tamura <i>et al.</i> [46]	WACV'19	34.8	72.1	27.7	51.7	38.8	8.7	38.8	32.9	34.2	72.8	28.7	53.7	37.3	6.5	39.5	33.2
RAPiD [9]	CVPRW'20	40.3	77.9	34.8	55.3	41.9	9.2	44.7	37.6	39.2	77.9	35.4	54.8	40.1	7.9	44.2	37.3
OARPD [33]	MTA'24	45.5	78.8	46.3	-	-	-	-	-	45.8	79.4	45.8	-	-	-	-	-
Yang <i>et al.</i> [63]	ICCV'23	47.4	82.6	48.4	64.1	<b>54.3</b>	14.1	50.8	45.7	46.2	81.1	47.3	66.1	<b>53.5</b>	<b>12.6</b>	49.3	44.9
Ours		<b>52.7</b>	<b>84.9</b>	<b>57.1</b>	<b>74.8</b>	51.6	<b>15.3</b>	<b>56.8</b>	<b>50.9</b>	<b>55.2</b>	<b>87.6</b>	<b>61.2</b>	<b>71.1</b>	51.8	9.8	<b>56.8</b>	<b>54.2</b>

**Table 4.** Ablation study on the LOAF test set

Method	test				
	mAP	AP <sub>50</sub>	AP <sub>75</sub>	AP <sub>seen</sub>	AP <sub>unseen</sub>
Baseline (DAB-DETR)	40.2	74.0	39.6	42.5	38.7
+ Panoramic conversion	50.6	85.2	54.1	52.1	49.8
+ PDAT	<b>55.2</b>	<b>87.6</b>	<b>61.2</b>	<b>56.8</b>	<b>54.2</b>

**Table 5.** Panoramic-image resolution analysis on the LOAF test set

Panorama width	test				
	mAP	AP <sub>50</sub>	AP <sub>75</sub>	AP <sub>seen</sub>	AP <sub>unseen</sub>
2048 pixel	46.9	81.5	47.9	47.9	46.2
2560 pixel	49.7	84.5	52.3	51.1	49.0
3072 pixel	<b>55.2</b>	<b>87.6</b>	<b>61.2</b>	<b>56.8</b>	<b>54.2</b>

#### 4.2.2. Diagnostic study

We conducted a diagnostic study on the LOAF test set. Table 4 shows the ablation study results. The baseline indicates DAB-DETR [26] with the SG-Former-S [36] for the backbones using fisheye input images. The second row demonstrates the effectiveness of the panoramic conversion. The panorama images were suitable for DAB-DETR because they removed person rotations. After adopting the panoramic conversion, the performance increased by an mAP of 10.4. We validated the effectiveness of the PDAT process. The third row indicates that our method using PDAT provided notably improved person detection results when compared with our method without the PDAT by an mAP of 4.6. Therefore, the PDAT alleviated the problems caused by the variations in person size dramatically. Similar to mAP, both AP<sub>seen</sub> and AP<sub>unseen</sub> were improved notably. In addition, Table 5 shows the dependency of the panoramic image width. The 3072-pixel panoramic image width is suitable for the 1024×1024-pixel fisheye images because the circumference of the fisheye image is  $\pi \times 1024 = 3217 \approx 3072$ . Therefore, the 3072-pixel image width without shrinkage led to the best performance among 2048, 2560, and 3072 pixels.

#### 4.2.3. Person localization

To validate the person localization accuracy, we compared our method with the conventional methods. We evaluated the individual person positions from the bounding boxes us-

ing Yang *et al.*'s approach [63], as described in Section 2. We defined the position error (PE) in meters as the horizontal distance between the ground-truth person position and the person position estimated from the bounding boxes. Our method achieved the lowest mean PE (mPE), as indicated in Table 6. The mPE for our method is smaller than that of Yang *et al.*'s method [63] on the LOAF test set by 0.069. Similar to the person detection performance, our method realized a noteworthy 0.122 gain in terms of the PE<sub>unseen</sub> when compared with Yang *et al.*'s method [63]. Our method outperformed the other methods on PE<sub>n</sub>, PE<sub>m</sub>, and PE<sub>f</sub> because of accurate bounding box detection.

#### 4.2.4. Qualitative evaluation

To evaluate the detection accuracy, we compared the bounding boxes. Figure 5(a) shows our detection results in a panoramic image on the LOAF test set. Although people at the top of the panoramic image are small, our networks can accurately detect bounding boxes. We found that some tiny persons without ground-truth annotations were also detected, as shown in the zoom-in area of Figure 5(a). Our network has the potential to detect more persons. Overall, our results are the closest to the ground-truth bounding boxes. Furthermore, the transformer-based methods proposed by Yang *et al.* [63] failed to detect some people at near image circles, as shown in Figure 5(b).

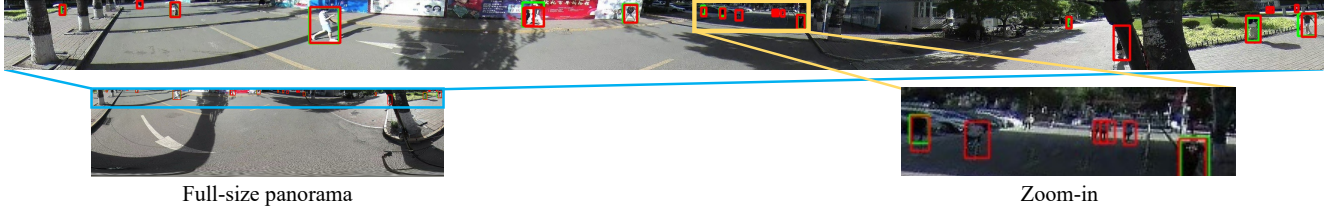
### 5. Conclusion

**Limitations.** We assume that the fisheye images are a stereographic projections. However, this assumption may cause a mismatch with the actual distortion. To address this problem, we will extend our method using a deep single image camera calibration technique [4, 53] that estimates the lens distortion. Another promising direction for future work is to use videos for the input. In this paper, we have focused on person detection and localization from an image.

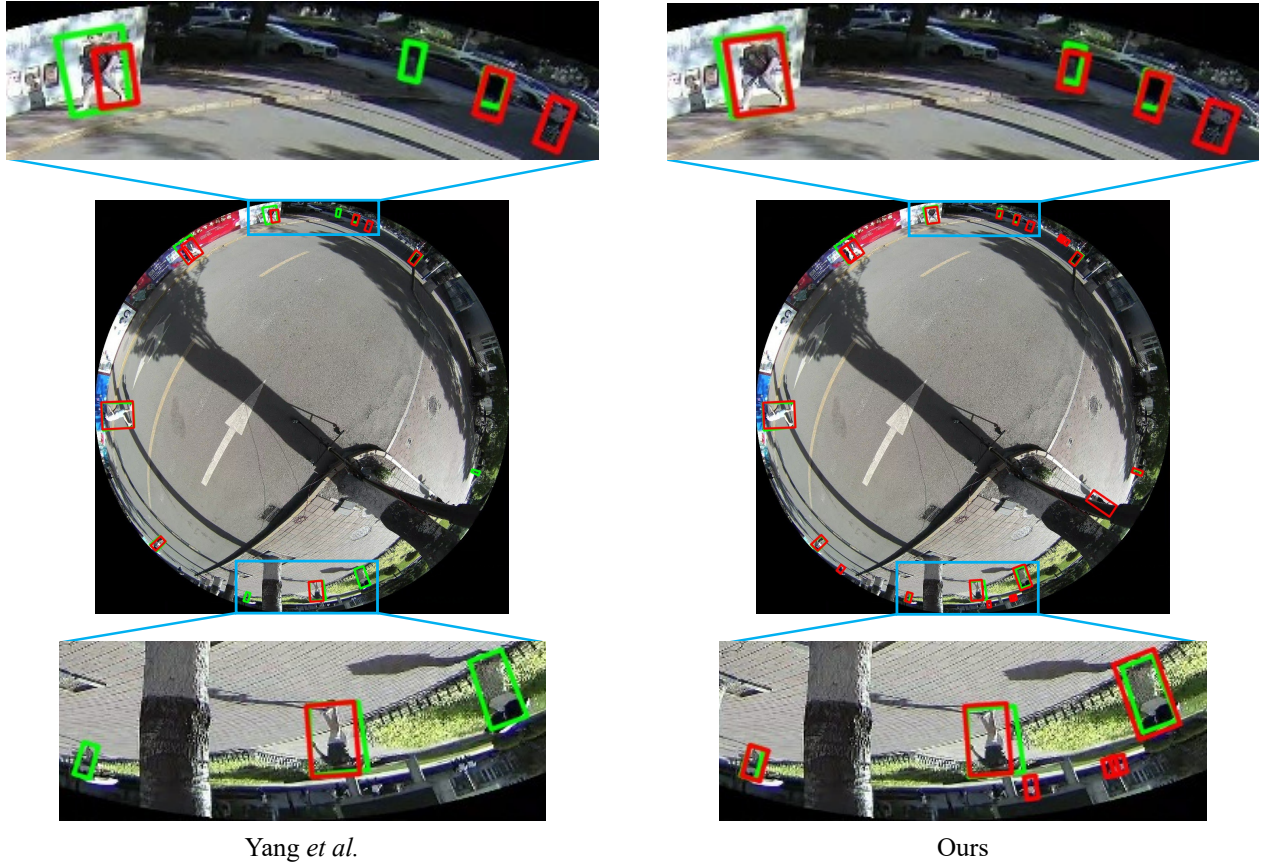
We have proposed a transformer-based detection and localization method for use with overhead fisheye images. Our nonuniform tokenization approach using self-similarity figures leverages the significance values to alleviate the imbalance in the significant areas of the feature maps. Extensive experiments demonstrated that our method outperforms the conventional methods substantially.

**Table 6.** Person localization results using position errors (PE) ↓ in meters on the LOAF validation (val) and test sets

Method	val						test						
	mPE	PE <sub>n</sub>	PE <sub>m</sub>	PE <sub>f</sub>	PE <sub>seen</sub>	PE <sub>unseen</sub>	mPE	PE <sub>n</sub>	PE <sub>m</sub>	PE <sub>f</sub>	PE <sub>seen</sub>	PE <sub>unseen</sub>	
Seidel <i>et al.</i> [40]	VISAPP'19	1.298	0.561	1.332	3.109	1.206	1.382	1.321	0.706	1.309	3.482	1.306	1.386
Li <i>et al.</i> [21]	AVSS'19	0.898	0.502	0.871	2.650	0.832	0.962	0.913	0.543	0.884	2.780	0.904	0.998
Tamura <i>et al.</i> [46]	WACV'19	0.755	0.429	0.736	1.862	0.709	0.821	0.778	0.471	0.826	2.160	0.724	0.836
RAPiD [9]	CVPRW'20	0.674	0.426	0.623	1.403	0.625	0.757	0.682	0.461	0.664	1.445	0.638	0.776
OARPD [33]	MTA'24	-	-	-	-	-	-	-	-	-	-	-	-
Yang <i>et al.</i> [63]	ICCV'23	0.368	0.144	0.363	0.775	0.318	0.402	0.374	0.148	0.375	0.819	<b>0.326</b>	0.398
Ours		<b>0.279</b>	<b>0.096</b>	<b>0.201</b>	<b>0.576</b>	<b>0.2695</b>	<b>0.306</b>	<b>0.305</b>	<b>0.117</b>	<b>0.253</b>	<b>0.598</b>	0.345	<b>0.276</b>



(a) Our detection result in a panoramic image



(b) Detection results in fisheye images

**Figure 5.** Qualitative results on the LOAF test set. Green and red rectangles indicate ground-truth and estimated bounding boxes, respectively. (a) Our detection result in a panoramic image. (b) From left to right: detection results of Yang *et al.* [63] and our method. For visualization, rotated rectangles are used for our method.



## References

- [1] D. Aiger, A. Araujo, and S. Lymen. Yes, we CANN: Constrained approximate nearest neighbors for local feature-based visual localization. In *Proceedings of the IEEE/CVF International Conference on Computer Vision (ICCV)*, pages 13293–13303, 2023. 3
- [2] A. Athwale, A. Afrasiyabi, J. Lagüe, I. Shili, O. Ahmad, and J.-F. Lalonde. DarSwin: Distortion aware radial swin transformer. In *Proceedings of the IEEE/CVF International Conference on Computer Vision (ICCV)*, pages 5906–5915, 2023. 4
- [3] V. Balntas, S. Li, and V. Prisacariu. RelocNet: Continuous metric learning relocalisation using neural nets. In *Proceedings of the European Conference on Computer Vision (ECCV)*, pages 782–799, 2018. 3
- [4] A. P. Dal Cin, F. Azzoni, G. Boracchi, and L. Magri. Revisiting calibration of wide-angle radially symmetric cameras. In *Proceedings of the European Conference on Computer Vision (ECCV)*, page 214–230, 2024. 7
- [5] C. R. del Blanco, P. Carballeira, F. Jaureguizar, and N. García. Robust people indoor localization with omnidirectional cameras using a grid of spatial-aware classifiers. *Signal Processing: Image Communication (SPIC)*, 93:116135, 2021. 2
- [6] P. Dollár, C. Wojek, B. Schiele, and P. Perona. Pedestrian detection: A benchmark. In *Proceedings of the IEEE Conference on Computer Vision and Pattern Recognition (CVPR)*, pages 304–311, 2009. 1
- [7] X. Dong, J. Bao, D. Chen, W. Zhang, N. Yu, L. Yuan, D. Chen, and B. Guo. CSWin Transformer: A general vision transformer backbone with cross-shaped windows. In *Proceedings of the IEEE/CVF Conference on Computer Vision and Pattern Recognition (CVPR)*, pages 12114–12124, 2022. 4
- [8] A. Dosovitskiy, L. Beyer, A. Kolesnikov, D. Weissenborn, X. Zhai, T. Unterthiner, M. Dehghani, M. Minderer, G. Heigold, S. Gelly, J. Uszkoreit, and N. Houlsby. An image is worth 16x16 words: Transformers for image recognition at scale. In *Proceedings of the International Conference on Learning Representations (ICLR)*, 2021. 3, 5
- [9] Z. Duan, M. Ozan Tezcan, H. Nakamura, P. Ishwar, and J. Konrad. RAPID: Rotation-aware people detection in overhead fisheye images. In *Proceedings of the IEEE/CVF Conference on Computer Vision and Pattern Recognition Workshops (CVPRW)*, pages 2700–2709, 2020. 2, 6, 7, 8
- [10] Z. Fu, Q. Liu, Z. Fu, and Y. Wang. STMTrack: Template-free visual tracking with space-time memory networks. In *Proceedings of the IEEE/CVF Conference on Computer Vision and Pattern Recognition (CVPR)*, pages 13774–13783, 2021. 1
- [11] H. Germain, V. Lepetit, and G. Bourmaud. Neural reprojection error: Merging feature learning and camera pose estimation. In *Proceedings of the IEEE/CVF Conference on Computer Vision and Pattern Recognition (CVPR)*, pages 414–423, 2021. 3
- [12] G. Ghiasi, Y. Cui, A. Srinivas, R. Qian, T.-Y. Lin, E. D. Cubuk, Q. V. Le, and B. Zoph. Simple copy-paste is a strong data augmentation method for instance segmentation. In *Proceedings of the IEEE/CVF Conference on Computer Vision and Pattern Recognition (CVPR)*, pages 2917–2927, 2021. 1, 3
- [13] Y. Gong, X. Yu, Y. Ding, X. Peng, J. Zhao, and Z. Han. Effective fusion factor in fpn for tiny object detection. In *Proceedings of the IEEE Winter Conference on Applications of Computer Vision (WACV)*, pages 1159–1167, 2021. 3
- [14] A. Hassani, S. Walton, J. Li, S. Li, and H. Shi. Neighborhood attention transformer. In *Proceedings of the IEEE/CVF Conference on Computer Vision and Pattern Recognition (CVPR)*, pages 6185–6194, 2023. 4
- [15] J. Hyeon, J. Kim, and N. Doh. Pose correction for highly accurate visual localization in large-scale indoor spaces. In *Proceedings of the IEEE/CVF International Conference on Computer Vision (ICCV)*, pages 15954–15963, 2021. 3
- [16] H. Ji, Z. Gao, X. Liu, Y. Zhang, and T. Mei. Small object detection leveraging on simultaneous super-resolution. In *Proceedings of the International Conference on Pattern Recognition (ICPR)*, pages 803–810, 2021. 3
- [17] A. Kendall, M. Grimes, and R. Cipolla. PoseNet: A convolutional network for real-time 6-DOF camera relocalization. In *Proceedings of the IEEE International Conference on Computer Vision (ICCV)*, pages 2938–2946, 2015. 3
- [18] A. H. Khan, M. S. Nawaz, and A. Dengel. Localized semantic feature mixers for efficient pedestrian detection in autonomous driving. In *Proceedings of the IEEE/CVF Conference on Computer Vision and Pattern Recognition (CVPR)*, pages 5476–5485, 2023. 1
- [19] A. Krizhevsky, I. Sutskever, and G. E. Hinton. ImageNet classification with deep convolutional neural networks. In *Proceedings of the Advances in Neural Information Processing Systems (NeurIPS)*, 2012. 2
- [20] B.-J. Lee, J. Choi, C. Baek, and B.-T. Zhang. Robust human following by deep bayesian trajectory prediction for home service robots. In *Proceedings of the IEEE International Conference on Robotics and Automation (ICRA)*, pages 7189–7195, 2018. 1
- [21] S. Li, M. Ozan Tezcan, P. Ishwar, and J. Konrad. Supervised people counting using an overhead fisheye camera. In *Proceedings of the IEEE International Conference on Advanced Video and Signal Based Surveillance (AVSS)*, pages 1–8, 2019. 2, 6, 7, 8
- [22] L. Lin, Y. Lu, Y. Pan, and X. Chen. Integrating graph partitioning and matching for trajectory analysis in video surveillance. *IEEE Transactions on Image Processing (TIP)*, 21(12):4844–4857, 2012. 1
- [23] T.-Y. Lin, M. Maire, S. Belongie, J. Hays, P. Perona, D. Ramanan, P. Dollár, and C. L. Zitnick. Microsoft COCO: Common objects in context. In *Proceedings of the European Conference on Computer Vision (ECCV)*, pages 740–755, 2014. 2, 6
- [24] T.-Y. Lin, P. Dollár, R. Girshick, K. He, B. Hariharan, and S. Belongie. Feature pyramid networks for object detection. In *Proceedings of the IEEE Conference on Computer Vision and Pattern Recognition (CVPR)*, pages 936–944, 2017. 2

- [25] K. Liu, Z. Fu, S. Jin, Z. Chen, F. Zhou, R. Jiang, Y. Chen, and J. Ye. ESOD: Efficient small object detection on high-resolution images. *IEEE Transactions on Image Processing (TIP)*, 34:183–195, 2025. 3
- [26] S. Liu, F. Li, H. Zhang, X. Yang, X. Qi, H. Su, J. Zhu, and L. Zhang. DAB-DETR: Dynamic anchor boxes are better queries for DETR. In *Proceedings of the International Conference on Learning Representations (ICLR)*, 2022. 2, 5, 6, 7
- [27] Z. Liu, Y. Lin, Y. Cao, H. Hu, Y. Wei, Z. Zhang, S. Lin, and B. Guo. Swin Transformer: Hierarchical vision transformer using shifted windows. In *Proceedings of the IEEE International Conference on Computer Vision (ICCV)*, pages 9992–10002, 2021. 4
- [28] M. López-Antequera, R. Marí, P. Gargallo, Y. Kuang, J. Gonzalez-Jimenez, and G. Haro. Deep single image camera calibration with radial distortion. In *Proceedings of the IEEE/CVF Conference on Computer Vision and Pattern Recognition (CVPR)*, pages 11809–11817, 2019. 3
- [29] I. Loshchilov and F. Hutter. Decoupled weight decay regularization. In *Proceedings of the International Conference on Learning Representations (ICLR)*, 2019. 6
- [30] B. Mandelbrot. How long is the coast of britain? statistical self-similarity and fractional dimension. *Science*, 156(3775): 636–638, 1967. 5
- [31] A. Paszke, S. Gross, F. Massa, A. Lerer, J. Bradbury, G. Chanan, T. Killeen, Z. Lin, N. Gimelshein, L. Antiga, A. Desmaison, A. Köpf, E. Yang, Z. DeVito, M. Raison, A. Tejani, S. Chilamkurthy, B. Steiner, L. Fang, J. Bai, and S. Chintala. PyTorch: An imperative style, high-performance deep learning library. In *Proceedings of the Advances in Neural Information Processing Systems (NeurIPS)*, pages 8024–8035, 2019. 6
- [32] E. Plaut, E. Ben Yaacov, and B. El Shlomo. 3D object detection from a single fisheye image without a single fish-eye training image. In *Proceedings of the IEEE/CVF Conference on Computer Vision and Pattern Recognition Workshops (CVPRW)*, pages 3654–3662, 2021. 3
- [33] R. Qiao, C. Cai, H. Meng, F. Wang, and J. Zhao. OARPD: Occlusion-aware rotated people detection in overhead fish-eye images. *Multimedia Tools and Applications (MTA)*, 83: 90375–90392, 2024. 2, 6, 7, 8
- [34] J. Redmon and A. Farhadi. YOLO9000: Better, faster, stronger. In *Proceedings of the IEEE Conference on Computer Vision and Pattern Recognition (CVPR)*, pages 6517–6525, 2017. 2
- [35] J. Redmon and A. Farhadi. YOLOv3: An incremental improvement. *arXiv preprint arXiv:1804.02767*, 2018. 2
- [36] S. Ren, X. Yang, S. Liu, and X. Wang. SG-Former: Self-guided transformer with evolving token reallocation. In *Proceedings of the IEEE/CVF International Conference on Computer Vision (ICCV)*, pages 5980–5991, 2023. 4, 5, 6, 7
- [37] O. Russakovsky, J. Deng, H. Su, J. Krause, S. Satheesh, S. Ma, Z. Huang, A. Karpathy, A. Khosla, M. Bernstein, A. C. Berg, and L. Fei-Fei. ImageNet large scale visual recognition challenge. *International Journal of Computer Vision (IJCV)*, 115(3):211–252, 2015. 6
- [38] P.-E. Sarlin, C. Cadena, R. Siegwart, and M. Dymczyk. From coarse to fine: Robust hierarchical localization at large scale. In *Proceedings of the IEEE/CVF Conference on Computer Vision and Pattern Recognition (CVPR)*, pages 12708–12717, 2019. 3
- [39] P.-E. Sarlin, A. Unagar, M. Larsson, H. Germain, C. Toft, V. Larsson, M. Pollefeys, V. Lepetit, L. Hammarstrand, F. Kahl, and T. Sattler. Back to the feature: Learning robust camera localization from pixels to pose. In *Proceedings of the IEEE/CVF Conference on Computer Vision and Pattern Recognition (CVPR)*, pages 3246–3256, 2021. 3
- [40] R. Seidel, A. Apitzsch, and G. Hirtz. Improved person detection on omnidirectional images with non-maxima suppression. In *Proceedings of the International Conference on Computer Vision Theory and Applications (VISAPP)*, 2019. 2, 6, 7, 8
- [41] A. Sharma and J. Ventura. Unsupervised learning of depth and ego-motion from cylindrical panoramic video. In *Proceedings of the IEEE International Conference on Artificial Intelligence and Virtual Reality (AIVR)*, pages 58–587, 2019. 5
- [42] J. Shermeyer and A. Van Etten. The effects of super-resolution on object detection performance in satellite imagery. In *Proceedings of the IEEE/CVF Conference on Computer Vision and Pattern Recognition Workshops (CVPRW)*, pages 1432–1441, 2019. 3
- [43] B. Singh and L. S. Davis. An analysis of scale invariance in object detection - SNIP. In *Proceedings of the IEEE/CVF Conference on Computer Vision and Pattern Recognition (CVPR)*, pages 3578–3587, 2018. 3
- [44] B. Singh, M. Najibi, and L. S. Davis. SNIPER: Efficient multi-scale training. In *Proceedings of the Advances in Neural Information Processing Systems (NeurIPS)*, pages 9310–9320, 2018. 3
- [45] H. J. S. Smith. On the integration of discontinuous functions. *Proceedings of the London Mathematical Society*, s1-6(1): 140–153, 1874. 5
- [46] M. Tamura, S. Horiguchi, and T. Murakami. Omnidirectional pedestrian detection by rotation invariant training. In *Proceedings of the IEEE Winter Conference on Applications of Computer Vision (WACV)*, pages 1989–1998, 2019. 2, 6, 7, 8
- [47] M. O. Tezcan, Z. Duan, M. Cokbas, P. Ishwar, and J. Konrad. WEPDToF: A dataset and benchmark algorithms for in-the-wild people detection and tracking from overhead fish-eye cameras. In *Proceedings of the IEEE/CVF Winter Conference on Applications of Computer Vision (WACV)*, pages 1381–1390, 2022. 2
- [48] A. Torii, H. Taira, J. Sivic, M. Pollefeys, M. Okutomi, T. Pajdla, and T. Sattler. Are large-scale 3D models really necessary for accurate visual localization? *IEEE Transactions on Pattern Analysis and Machine Intelligence (PAMI)*, 43(3): 814–829, 2021. 3
- [49] Z. Tu, H. Talebi, H. Zhang, F. Yang, P. Milanfar, A. Bovik, and Y. Li. MaxViT: Multi-axis vision transformer. In *Proceedings of the European Conference on Computer Vision (ECCV)*, page 459–479, 2022. 4

- [50] F. Ö. Ünel, B. O. Özkalayci, and C. Çiğla. The power of tiling for small object detection. In *Proceedings of the IEEE/CVF Conference on Computer Vision and Pattern Recognition Workshops (CVPRW)*, pages 582–591, 2019. 3
- [51] R. Varghese and S. M. YOLOv8: A novel object detection algorithm with enhanced performance and robustness. In *Proceedings of the International Conference on Advances in Data Engineering and Intelligent Computing Systems (ADICS)*, pages 1–6, 2024. 2
- [52] A. Vaswani, N. Shazeer, N. Parmar, J. Uszkoreit, L. Jones, A. N. Gomez, Ł. Kaiser, and I. Polosukhin. Attention is all you need. In *Proceedings of the Advances in Neural Information Processing Systems (NeurIPS)*, pages 6000–6010, 2017. 2
- [53] N. Wakai, S. Sato, Y. Ishii, and T. Yamashita. Rethinking generic camera models for deep single image camera calibration to recover rotation and fisheye distortion. In *Proceedings of the European Conference on Computer Vision (ECCV)*, pages 679–698, 2022. 5, 7
- [54] N. Wakai, S. Sato, Y. Ishii, and T. Yamashita. Deep single image camera calibration by heatmap regression to recover fisheye images under manhattan world assumption. In *Proceedings of the IEEE/CVF Conference on Computer Vision and Pattern Recognition (CVPR)*, pages 11884–11894, 2024. 3
- [55] F. Walch, C. Hazirbas, L. Leal-Taixe, T. Sattler, S. Hilsenbeck, and D. Cremers. Image-based localization using LSTMs for structured feature correlation. In *Proceedings of the IEEE International Conference on Computer Vision (ICCV)*, pages 627–637, 2017. 3
- [56] F.-E. Wang, Y.-H. Yeh, M. Sun, W.-C. Chiu, and Y.-H. Tsai. LED2-Net: Monocular 360° layout estimation via differentiable depth rendering. In *Proceedings of the IEEE/CVF Conference on Computer Vision and Pattern Recognition (CVPR)*, pages 12951–12960, 2021. 3
- [57] J. Wang, K. Sun, T. Cheng, B. Jiang, C. Deng, Y. Zhao, D. Liu, Y. Mu, M. Tan, X. Wang, W. Liu, and B. Xiao. Deep high-resolution representation learning for visual recognition. *IEEE Transactions on Pattern Analysis and Machine Intelligence (PAMI)*, 43(10):3349–3364, 2021. 3
- [58] W. Wang, J. Dai, Z. Chen, Z. Huang, Z. Li, X. Zhu, X. Hu, T. Lu, L. Lu, H. Li, X. Wang, and Y. Qiao. InternImage: Exploring large-scale vision foundation models with deformable convolutions. In *Proceedings of the IEEE/CVF Conference on Computer Vision and Pattern Recognition (CVPR)*, pages 14408–14419, 2023. 1
- [59] Wenxiao Wang, Wei Chen, Qibo Qiu, Long Chen, Boxi Wu, Binbin Lin, Xiaofei He, and Wei Liu. CrossFormer++: A versatile vision transformer hinging on cross-scale attention. *IEEE Transactions on Pattern Analysis and Machine Intelligence (PAMI)*, 46(5):3123–3136, 2024. 4
- [60] Z. Xia, X. Pan, S. Song, L. E. Li, and G. Huang. Vision transformer with deformable attention. In *Proceedings of the IEEE/CVF Conference on Computer Vision and Pattern Recognition (CVPR)*, pages 4784–4793, 2022. 4
- [61] Y. Xie, L. Lin, and Y. Jia. Tracking objects with adaptive feature patches for PTZ camera visual surveillance. In *Proceedings of the International Conference on Pattern Recognition (ICPR)*, pages 1739–1742, 2010. 1
- [62] L. Yang, Z. Bai, C. Tang, H. Li, Y. Furukawa, and P. Tan. SANet: Scene agnostic network for camera localization. In *Proceedings of the IEEE/CVF International Conference on Computer Vision (ICCV)*, pages 42–51, 2019. 3
- [63] L. Yang, L. Li, X. Xin, Y. Sun, Q. Song, and W. Wang. Large-scale person detection and localization using overhead fisheye cameras. In *Proceedings of the IEEE/CVF International Conference on Computer Vision (ICCV)*, pages 19904–19914, 2023. 1, 2, 3, 5, 6, 7, 8
- [64] T. Yoshimi, M. Nishiyama, T. Sonoura, H. Nakamoto, S. Tokura, H. Sato, F. Ozaki, N. Matsuhira, and H. Mizoguchi. Development of a person following robot with vision based target detection. In *Proceedings of the IEEE/RSJ International Conference on Intelligent Robots and Systems (IROS)*, pages 5286–5291, 2006. 1
- [65] X. Yu, Y. Gong, N. Jiang, Q. Ye, and Z. Han. Scale match for tiny person detection. In *Proceedings of the IEEE Winter Conference on Applications of Computer Vision (WACV)*, pages 1246–1254, 2020. 3
- [66] T. Yuan, X. Zhang, K. Liu, B. Liu, C. Chen, J. Jin, and Z. Jiao. Towards surveillance video-and-language understanding: New dataset, baselines, and challenges. In *Proceedings of the IEEE/CVF Conference on Computer Vision and Pattern Recognition (CVPR)*, pages 22052–22061, 2024. 1
- [67] D. Zhang, L. Birner, F. Pancheri, C. Rehekampff, D. Burschka, and T. C. Lueth. A hybrid human tracking system using UWB sensors and monocular visual data fusion for human following robots. In *Proceedings of the IEEE/RSJ International Conference on Intelligent Robots and Systems (IROS)*, pages 10878–10883, 2024. 1
- [68] S. Zhang, R. Benenson, M. Omran, J. Hosang, and B. Schiele. Towards reaching human performance in pedestrian detection. *IEEE Transactions on Pattern Analysis and Machine Intelligence (PAMI)*, 40(4):973–986, 2018. 1
- [69] L. Zhu, X. Wang, Z. Ke, W. Zhang, and R. Lau. BiFormer: Vision transformer with bi-level routing attention. In *Proceedings of the IEEE/CVF Conference on Computer Vision and Pattern Recognition (CVPR)*, pages 10323–10333, 2023. 4
- [70] P. Zhu, L. Wen, X. Bian, H. Ling, and Q. Hu. Vision meets drones: A challenge. *arXiv preprint arXiv:1804.07437*, 2018. 3
- [71] X. Zhu, W. Su, L. Lu, B. Li, X. Wang, and J. Dai. Deformable DETR: Deformable transformers for end-to-end object detection. In *Proceedings of the International Conference on Learning Representations (ICLR)*, 2021. 5
- [72] Z. Zong, G. Song, and Y. Liu. DETRs with collaborative hybrid assignments training. In *Proceedings of the IEEE/CVF International Conference on Computer Vision (ICCV)*, pages 6725–6735, 2023. 1